Neuron, Vol. 17, 1251–1264, December, 1996, Copyright ©1996 by Cell Press

Inner Ear Defects Induced by Null Mutation of the *isk* Gene

Douglas E. Vetter,* Jeffrey R. Mann,†#
Philine Wangemann,‡# Jianzhong Liu,‡
K. John McLaughlin,† Florian Lesage,§
Daniel C. Marcus,‖ Michel Lazdunski,§
Stephen F. Heinemann,* and Jacques Barhanin§
*The Salk Institute for Biological Studies
La Jolla, California
†Beckman Research Institute of the City of Hope
Duarte, California
‡Cell Physiology Laboratory
Boystown National Research Hospital
Omaha, Nebraska
§CNRS Institut de Pharmacologie Moleculaire et Cellulaire
Valbonne
France
‖Biophysics Laboratory
Boystown National Research Hospital
Omaha, Nebraska

Summary

The *isk* gene is expressed in many tissues. Pharmacological evidence from the inner ear suggests that Isk mediates potassium secretion into the endolymph. To examine the consequences of *IsK* null mutation on inner ear function, and to produce a system useful for examining the role(s) IsK plays elsewhere, we have produced a mouse strain that carries a disrupted *isk* locus. Knockout mice exhibit classic shaker/waltzer behavior. Hair cells degenerate, but those of different inner ear organs degenerate at different times. Functionally, we show that in mice lacking *isk*, the strial marginal cells and the vestibular dark cells of the inner ear are unable to generate an equivalent short circuit current in vitro, indicating a lack of transepithelial potassium secretion.

Introduction

Potassium (K^+) channels are found in most excitable and nonexcitable mammalian cells, and can be divided into a number of distinct families based on structural features. All cloned K^+ channels have in common multiple transmembrane domains as well as a P-domain, shown to be an essential element of the K^+ selective pore and considered to be the signature of a K^+ channel structure (Doupnik et al., 1995; Heginbotham et al., 1994; Jan and Jan, 1994; Lesage et al., 1996; Li et al., 1994; MacKinnon, 1995; Pascual et al., 1995; Pongs, 1992, 1993). In addition to, but distinct from, these K^+ channel families is the IsK protein, which induces a slowly activating voltage-dependent K^+ current when expressed in Xenopus oocytes (Takumi et al., 1988). Recent evidence has been obtained showing that IsK is not capable of acting alone, but coassembles with the protein encoded by the KvLQT1 gene (Barhanin et al., 1996; Sanguinetti et al., 1996), a structurally more classical K^+ channel subunit. It is unknown at this time whether IsK can coassemble with other K^+ channel subunits (for simplicity, the channel(s) that coassemble with IsK are referred to herein as the IsK channel). The IsK protein is small (129 amino acids in mouse), contains a single putative transmembrane domain, and has no sequence homology with other cloned channels. The physiology of the IsK channel is also distinct from that of the other cloned K^+ channels (for review, see Swanson et al., 1993). IsK currents are small and slowly activating and deactivating. Activation develops following a delay once the cells are depolarized positive to −50 mV. The time course of the IsK current is voltage dependent, and deactivation can typically require seconds to complete. Single channel conductance is unusually small and has been estimated to be on the order of 1–6 pS in native inner ear and heart cells (Freeman and Kass, 1993; Shen et al., 1996; Tohse, 1990).

The IsK channel is also pharmacologically unique with respect to the other cloned K^+ channels. Thus, while some compounds that typically block other K^+ channels can also block the IsK channel at high concentrations (for review, see Swanson et al., 1993), many blockers of other K^+ channels have no effect (Honore et al., 1991). The IsK channel is blocked by some class III anti-arrhythmic drugs (Folander et al., 1990; Honore et al., 1991; Busch et al., 1994, 1996; Shen et al., 1996), and this, in combination with its coassembly with KvLQT1, has fueled speculation of a role for IsK in heart arrhythmia.

IsK is expressed in many mammalian tissues, including the kidney (Takumi et al., 1988), duodenum (Takumi et al., 1988), T-lymphocytes (Attali et al., 1992), uterus (Felipe et al., 1994; Folander et al., 1990), submandibular salivary glands (Sugimoto et al., 1990), heart (Folander et al., 1990; Honore et al., 1991), retinal large ganglion neurons (Tsukahara et al., 1995), corneal epithelial cells (Tsukahara et al., 1995), and inner ear (Sakagami et al., 1991). In epithelial cells that express IsK, the protein is compartmentalized to the apical membrane (Sugimoto et al., 1990). Thus far, a functional role for IsK has only been suggested in the heart and the inner ear. In the heart, the extensive similarities between IsK currents expressed in Xenopus oocytes and I_{Ks} currents measured in ventricular cells hint at the possibility that IsK underlies the very slow component of the cardiac delayed rectifier I_K current (for review, see Swanson et al., 1993). In the inner ear, IsK is located in the marginal cells of the stria vascularis in the cochlear duct and in the vestibular dark cells, and seems to be responsible for transporting high concentrations of K^+ into the fluid bathing the hair cell hair bundles (Marcus and Shen, 1994; Shen et al., 1996; Wangemann et al., 1995a), thus effectively creating a specialized extracellular fluid, the endolymph, and establishing the ionic environment necessary for normal hair cell transduction.

To investigate further and more directly the role of the IsK protein in different tissues in vivo, we used a gene-targeting strategy to generate a mouse strain that has

#These authors contributed equally to the project reported in this paper.

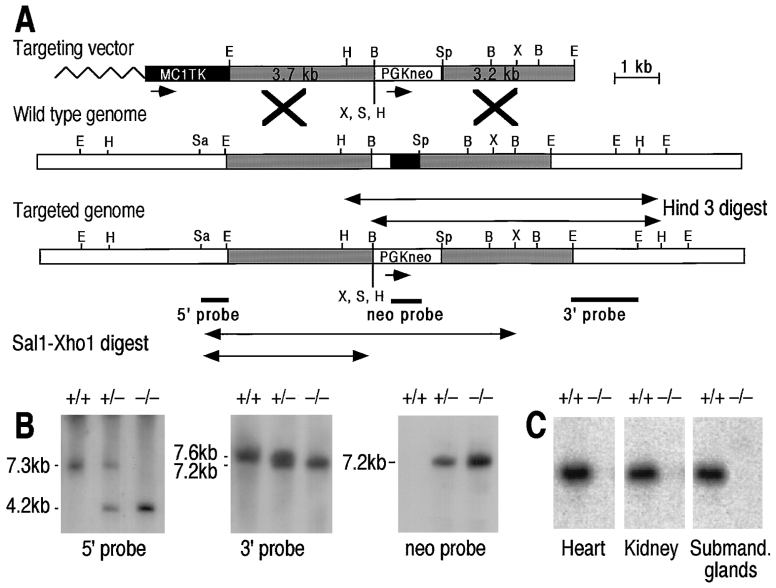

Figure 1. Targeted Disruption of the *isk* Gene

(A) Gene structures and restriction maps for the *isk* targeting construct, wild-type, and recombinant alleles are shown. The black box represents the region of exon 2 containing the entire coding sequence included in the BamH1–Sph1 fragment that is replaced by the neomycin resistance gene (pGKneo). The herpes virus thymidine kinase gene (MC1 TK) is attached to the 5′ end of the targeting vector for negative selection. Restriction sites are: BamHI (B), EcoRI (E), HindIII (H), SalI (Sa), SphI (S), and XhoI (X). The locations of the 5′- and 3′-flanking probes and of the neo probe are shown as thick lines, and arrows indicate the SalI–EcoRI and HindIII restriction fragment sizes for wild-type and rcombinant DNA.

(B) Southern blot analysis of genomic DNA of wild-type (+/+), heterozygous (+/−), and homozygous (−/−) mutant mice. SalI–EcoRI-digested DNA was hybridized with the 5′ probe to reveal the 7.3 kb (wild type) and 4.2 kb (recombinant) bands; HindIII-digested DNA was hybrized with the 3′ probe to reveal the 7.6 kb (wild type) and 7.2 kb (recombinant) bands and with the neo probe to confirm the presence of only one band of the expected 7.2 kb size in +/− and −/− animals.

(C) Absence of PCR amplified *isk* transcript in heart, kidney, and submandibular gland mRNA from mutant mice. After PCR, reaction products were prepared for Southern blot and probed with a specific radiolabeled *isk* cDNA.

a highly specific and complete loss of the *isk* gene product. In this paper, we describe the generation of the *isk* null mutant mice and document the resultant morphological and physiological consequences in the inner ear.

Results

Generation and Analysis of *isk* Mutant Mice

The gene encoding mouse IsK was cloned from a mouse 129/Sv DNA genomic library. An 8.1 kb fragment, which contained the entire exon 2, which itself contains the full uninterrupted coding sequence for IsK (Lesage et al., 1992), was used for constructing the targeting vector. The entire coding sequence, included in a 1.2 kb BamH1–Sph1 fragment, was deleted in the targeting vector and replaced by the neomycin resistance gene (Figure 1A). Following electroporation and selection (see Experimental Procedures), clones were screened by Southern blot hybridization using three probes, one specific to a region 5′ to the site of recombination, one specific to the neo cassette itself, and one specific to a region 3′ to the site of recombination (data not shown). Two of the correctly targeted clones were injected into C57Bl/6J blastocysts to produce chimeras, one of which was then mated with 129/Sv wild-type females. Resultant heterozygotes (identified by PCR analysis) were bred to obtain homozygotes. Southern blotting on liver DNA from wild type, heterozygous, and homozygous mutants confirmed that there were no gross rearrangements, deletions, or secondary integrations of the targeting sequence (Figure 1B). Digestion with Sal1 and Xho1 yielded a 7.3 kb band product from the wild-type locus when hybridized with the 5′ probe, while the correctly targeted locus yielded the predicted 4.2 kb band product. Following restriction enzyme digestion with Hind3 and hybridization with the neo-specific probe, only targeted loci yielded a hybridization product, the predicted 7.1 kb band. Finally, when a Southern analysis employing the 3′ specific probe was performed on the results of a Hind3 digest, the correctly targeted locus yielded the predicted 7.2 kb band product, while the wild-type locus yielded a 7.6 kb band. A PCR analysis using primers specific for the *isk* mRNA confirmed its total absence in mRNA from the tissues known to be the richest sources for this message, including submandibular salivary glands, heart, and kidney (Honore et al., 1991; Sugimoto et al., 1990) (Figure 1C). Thus, the effectiveness of the *isk* gene knockout was demonstrated at both the DNA and mRNA levels.

Gross Behavioral Characterization of *isk* Null Mutant (*isk* −/−) Mice

Mouse pups carrying one or two null allele mutations of the *isk* gene (*isk* +/− and *isk* −/−, respectively) were normal in appearence. However, *isk* −/− pups had difficulty righting themselves, but this disappeared as the animals matured. Additional locomotor deficits became evident with age. At an age when wild-type and *isk* +/− mice began to walk steadily, *isk* −/− mice exhibited an awkward uncoordinated movement. The *isk* −/− mice exhibited hyperactivity, and usually showed rapid head bobbing and occassionally a head tilt. More mature *isk* −/− mice displayed an intermittant bidirectional circling behavior, which became the overt behavioral phenotype displayed throughout life. The bidirectional circling, hyperactivity, head bobbing, and head tilt behaviors are characteristic of mouse mutants with inner ear defects, and is commonly referred to as a Shaker/waltzer phenotype (Deol, 1968). Upon examination for a Preyer's reflex, *isk* −/− mice failed to show any pinnea reflex or even signs of startle. Both wild-type and *isk* +/− mice exhibited a normal Preyer's reflex and startle response.

The mutant mice and their littermate controls were also tested for their swimming ability. When placed into

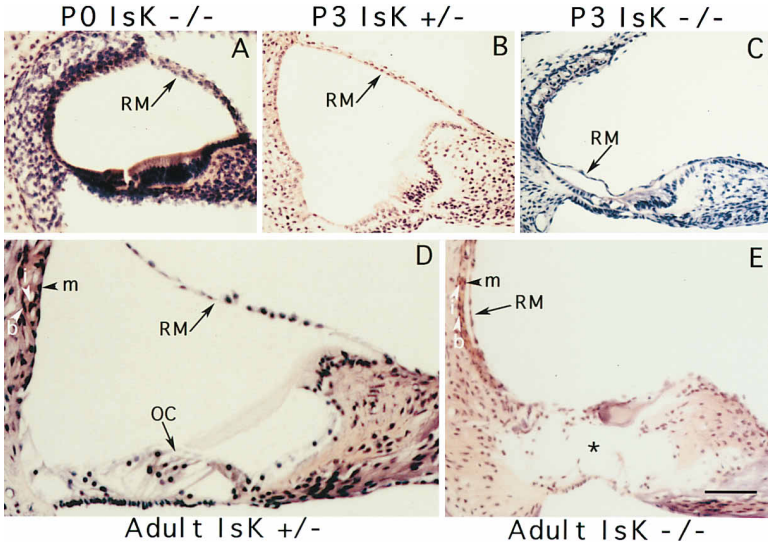

Figure 2. Position of Reissner's Membrane

(A) Reissner's membrane (RM) is distended normally over the scala media in P0 *isk* −/− mice. Similar observations were made in wild-type and *isk* +/− mice (data not shown).

(B) RM is normally situated over the spiral limbus in P3 *isk* +/− mice.

(C) RM has collapsed onto the top of the tectorial membrane and can be observed along the reticular laminar and lateral wall of the cochlear duct in P3 *isk* −/− mice

(D) RM is normally positioned in adult *isk* +/− mice (approximately 1 month old). The organ of Corti (OC) is normal, and the stria vascularis exhibits three cell layers.

(E) RM remains collapsed in adult *isk* −/− mice. The organ of Corti (*) is also degenerated. However, the stria vascularis is still composed of three cell layers, and thus seems to not be undergoing degenerative changes. MC, marginal cell; IC, intermediate cell; BC, basal cell. Scale bar, 200 μm.

a deep tank filled with ambient temperature water, *isk* −/− mice immediately began rotating along their long axis, and sank underwater. While underwater, the mice also began somersaulting, while still rotating along their body length. The mice seldom resurfaced, and after 30 s were rescued. Both wild-type and *isk* +/− mice exhibited normal swimming behavior for the 30 s test.

The gross behavioral phenotype exhibited by *isk* −/− mice suggested that the inner ear was in some way compromised by knocking out the *isk* gene. Therefore, this paper details the anatomical structure and physiological functioning of the inner ear in *isk* −/− mice.

Cochlea

Reissner's Membrane Collapse

The scala media (also referred to as the endolymphatic space) contains the high K^+ low Na^+ endolymphatic fluid, and is enclosed and separated from scala vestibuli and scala tympani by an epithelial lining contributed by Reissner's membrane, the reticular lamina, and various supporting epithelial cells. The position of Reissner's membrane has been used as an indication of intracochlear fluid pressure (Belal and Ylikoski, 1980). Pharmacological evidence suggests that K^+ diffuses passively into the endolymphatic space from the marginal cells of the stria vascularis via IsK channels (Shen et al., 1996; Wangemann et al., 1995a). Therefore, if IsK would be essential and sufficient for K^+ secretion, one would predict that by knocking out the *isk* gene, and hence the expression of the IsK channel, endolymph would not be produced, as K^+ and its associated water would not diffuse into scala media. Since there is an active reabsorption process in the inner ear, any fluid in the endolymphatic space would slowly shrink in volume, and Reissner's membrane would finally "collapse" under the influence of the fluid pressure in the scala vestibuli.

The developmental time course of the generation and maintenance of the scala media and the position of Reissner's membrane was examined (Figure 2). At P0 (defined as the first 24 hr after birth), Reissner's membrane appeared morphologically normal and its position in the cochlea was normal in *isk* −/− mice (Figure 2A), as well as in *isk* +/− and wild-type littermate controls (data not shown). At P3, however, the position of Reissner's membrane changed in *isk* −/− mice. While in the wild type (data not shown) and *isk* +/− littermate controls (Figure 2B) the position of Reissner's membrane was normal, in *isk* −/− mice, Reissner's membrane was collapsed onto the surface of the spiral limbus, along the tectorial membrane and reticular lamina, and along the lateral wall of the cochlea in close apposition to the stria vascularis (Figure 2C). The collapse of Reissner's membrane was irreversible, as all other ages examined (P7, 10, 20, 42 [Figures 2D and 2E], 3 months old, 5 months old, and 7 months old) exhibited the same pathology.

Hair Cell Death

The hair cells of the cochlear duct differentiated normally, but then degenerated postnatally in *isk* −/− mice. Both *isk* +/− and wild-type littermates exhibited normal embryonic and postnatal development. The normal development of the inner ear has already been described in detail (Sher, 1971).

The cochlea of *isk* +/− and *isk* −/− mice are illustrated in Figure 3. At E17.5, both outer and inner hair cells were clearly discernible among the various other cells present. Cochleas from both *isk* +/− (Figure 3A) and *isk* −/− (Figure 3B) mice contained a normally differentiated sensory epithelium. Similarly, at P0 the outer and inner hair cells were still present and viable in both *isk* +/− and *isk* −/− mice. However, at P3, the time when Reissner's membrane was first observed to have collapsed (Figure 2C), a change in the structure of the sensory epithelium was observed between the *isk* +/− and *isk* −/− mice. While the P3 heterozygous mice exhibited continued normal development of the organ of Corti, which includes the sensory hair cells and their associated supporting cells (Figure 3E), *isk* −/− mice exhibited degeneration of the organ of Corti in all turns of the cochlea (Figure 3F). Cellular debris was evident in regions of degeneration. Interestingly, the degeneration seemed not to include the supporting cells outside the organ of Corti at this early stage, nor did the degeneration spread to include cells within the developing spiral

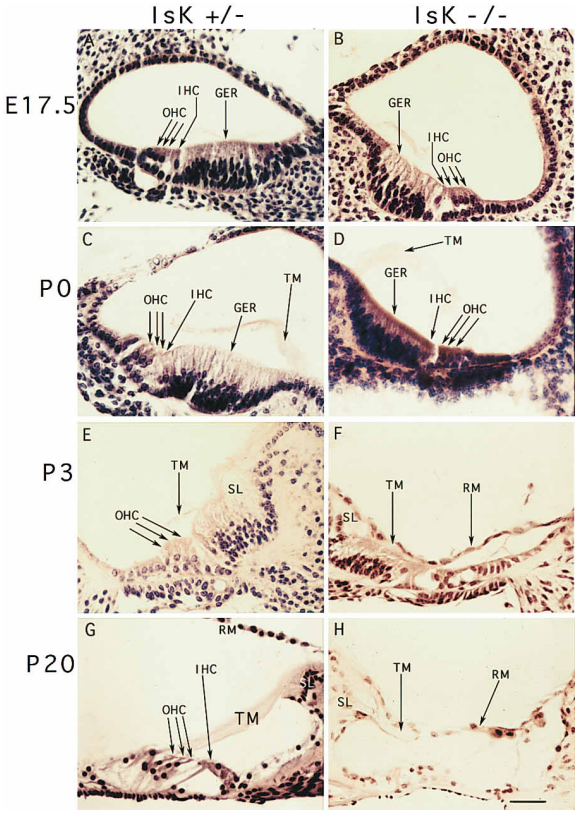

Figure 3. Hair Cell Death in the Cochlea

(A) Newly differentiated inner and outer hair cells (IHC and OHC) are apparent above a single cell layer adjacent to the greater epithelial ridge (GER) of E17.5 *isk* +/− mice.

(B) Differentiated IHCs and OHCs can be observed in their correct location in E17.5 *isk* −/− mice.

(C) IHCs and OHCs are readily apparent at P0 in *isk* +/− mice.

(D) IHCs and OHCs are still evident in *isk* −/− mice at P0.

(E) At P3 in *isk* +/− mice, the organ of Corti continues to develop, and the spiral limbus (SL) begins to take on a more mature profile.

(F) Hair cells in the organ of Corti of P3 *isk* −/− mice have begun to degenerate and Reissner's membrane has collapsed onto the tectorial membrane and reticular lamina. Note, however, that the spiral limbus seems to be unaffected.

(G) Both IHCs and OHCs of P20 *isk* +/− mice appear normal.

(H) By P20 in *isk* −/− mice, the vast majority of cellular debris left behind in the organ of Corti has been cleared. The spiral limbus seems to be normally developed, while the tectorial membrane appears somewhat shrunken and Reissner's membrane remains collapsed. GER, greater epithelial ridge; IHC, inner hair cell; OHC, outer hair cell; RM, Reissner's membrane; SL, spiral limbus; TM, tectorial membrane. Scale bar, 100 μm.

sulcus or spiral limbus. At P20, hair cells and supporting cells were readily evident in *isk* +/− mice (Figure 3G). The cochleas of P20 *isk* −/− mice, however, did not contain an organ of Corti (Figure 3H). No cellular debris was observed. Many supporting cells normally located laterally also degenerated, although the extent of degeneration was somewhat variable between animals. However, other regions of the cochlea continued to develop normally. Thus, the spiral sulcus and spiral limbus took on a more mature profile (Figure 3H).

Spiral Ganglion Cell Death

Neither wild-type nor *isk* +/− littermate controls showed an observable loss of spiral ganglion cells. By contrast, spiral ganglion cells in *isk* −/− mice degenerated. To assess the degree to which the spiral ganglion cells degenerated, ganglion cell profiles were counted in all turns of the cochlea at ages P7 and P42. There was no significant difference in the number of spiral ganglion cell profiles from age- and level-matched regions of cochleas between wild-type mice and *isk* +/− mice (data not shown). No signs of spiral ganglion cell death were evident in level-matched regions of cochleas between *isk* +/− and *isk* −/− mice at P7 (Figure 4C). The first signs of spiral ganglion cell degeneration were observed at P20 as occasional vacuoles present in the ganglion (data not shown). However, the variability was high between groups at this age and, thus, no statistically significant changes could be found (data not shown). At the next age examined, P42, the great majority of spiral ganglion cells in the base and middle turns of the cochlea had degenerated (compare Figures 4A and 4B). The greatest loss of cells occurred in the basal turn of the cochlea, while there was less loss in the middle turns and there was no significant loss of ganglion cells in the apex (Figure 4D), despite the fact that the degeneration of hair cells within the cochlea was complete throughout all turns of the cochlea. No loss of apical ganglion cells was observed even in 7-month-old *isk* −/− mice (data not shown).

Stria Vascularis

At the light microscopic level, three layers of cell nuclei in the SV were identifiable in wild-type, *isk* +/− (Figure 2D), and *isk* −/−mice (Figure 2E). However, while basal cells could be identified, it was difficult to discern marginal and intermediate cells. While no consistent changes in the SV were observed in *isk* −/− mice, an electron microscopic examination of the adult SV from an *isk* +/− and an *isk* −/− mouse was performed to rule out any possible changes undetectable at the light microscopic level.

At the EM level, all three SV cell types (Hinojosa and Rodriguez-Echandia, 1966) were identified in both *isk* +/− and *isk* −/− mice (Figures 5A and 5B). In addition, there was no observable difference in the structure or gross number of SV blood vessels between these animals. However, *isk* −/− mouse exhibited an expansion of the intercellular space between marginal and intermediate cell processes, and between marginal cell processes and blood vessels (Figures 5B and 5D). The expansion of the intercellular space surrounding marginal cell extensions was evident throughout the entire intermediate cell layer. In addition, intermediate cells often appeared vacuolated, but no cellular debris was observed, suggesting that while the intermediate cells were compromised morphologically, no massive cell death had occurred.

Vestibular Labyrinth

Vestibular Wall Collapse

Given that *isk* −/− mice exhibited behavior consistent with vestibular dysfunction, the vestibular labyrinth of *isk* −/− mice, as well as their *isk* +/− and wild-type littermates, were examined. At P3, the age at which Reissner's membrane collapsed in the cochlea, wild-type and *isk* +/− mice exhibited a normal vestibular wall in the utricle, sacculus, and crista ampullaris (Figure

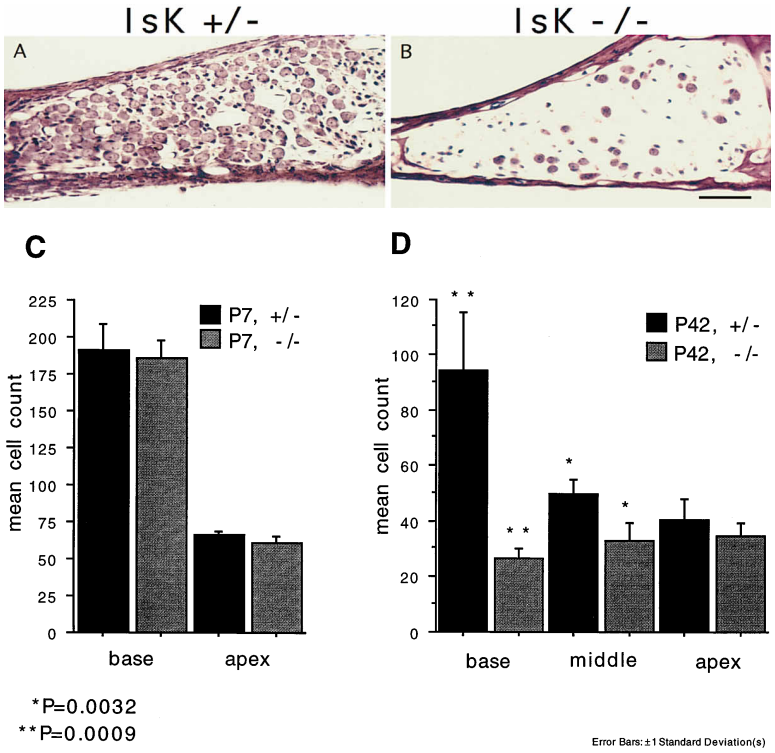

Figure 4. Spiral Ganglion Cell Death

(A) Spiral ganglion from the basal turn of the cochlea of a P42 *isk* +/− mouse. The normal complement of cells is found.

(B) Spiral ganglion from the basal turn of the cochlea of a P42 *isk* −/− mouse. Massive cell death has occurred, and only a few scattered cells remain. Scale bar, 100 μm.

(C) Spiral ganglion cell profiles were counted in the base and the apex of P7 *isk* +/− and *isk* −/− mice (see Experimental Procedures for details). No statistical differences exist between the numbers of profiles counted at this age.

(D) Spiral ganglion cell profiles were counted in the base and the apex of P7 *isk* +/− and *isk* −/− mice (see Experimental Procedures for details). There were significantly less spiral ganglion cell profiles in the basal ($P = 0.0009$) and middle ($P = 0.0032$) turns of the cochleas of *isk* −/− mice compared with their littermate controls. No statistically relevant differences were observed between the animal groups in the apical regions of the cochlea.

6A), while *isk* −/− mice exhibited a crenation or collapse of the wall (Figure 6B), indicating a decrease in endolymph volume. Mirroring the condition in the cochlear duct, the collapse of the vestibular wall was irreversible throughout the vestibule, as illustrated in the sacculus at different ages (Figures 6C and 6D). The position of the vestibular wall was normal in both wild-type and *isk* +/− mice throughout adulthood.

Hair Cell Death

The vestibular labyrinths of wild-type, *isk* +/−, and *isk* −/− mice at various ages (P0, 3, 7, 10, 20, 42, 3 months, 5 months, and 7 months) were examined for degenerating hair cells. Hair cell degeneration was not observed in *isk* +/− or wild-type mice. In the utricle (data not shown) and the saccule (Figure 6D) of *isk* −/− mice, hair cell degeneration was not observed during early adulthood (up to 3 months of age). However, at 5 months of age, the macula of the sacculus showed signs of slight degeneration, and by 7 months of age, the macula had undergone complete degeneration of both Types I and II hair cells and contained only support cells (data not shown). However, hair cell death did occur relatively early in the cristae, although the time course of degeneration was different from that observed in the cochlea. At P0, the cristae of *isk* −/− mice appeared normal (Figure 7A). At P3, a time when hair cells in the cochlea had degenerated, both Type I and Type II hair cells of the cristae still appeared normal (Figure 6B). The first signs of hair cell degeneration in the cristae began at approximately P10 (Figure 7B). At this age, vacuoles were observed within the sensory epithelium and in the supporting cell layer, but little change was observed in the region containing the afferent and efferent nerves. No differential susceptibility was observed between hair cell types. By P42 (Figure 7C), the cristae were observed undergoing massive degeneration. In addition to hair cells, the transitional epithelium and the inner core of the cristae were degenerating. Usually, the melanocyte and dark cell layer was twisted and displaced toward the epithelial surface of the cristae. There was also a loss of connective tissue that normally underlies the entire vestibular structure. Finally, after more than two months of age, the cristae appeared as an empty shell (Figure 7D), with only scattered cells along the basal, lateral, and apical surfaces. By 7 months of age, no structure could be discerned within the ampullae (data not shown). All three cristae were equally involved in this process.

Vestibular Dark Cell Degeneration

The vestibular dark cells are homologous to the marginal cells of the stria vascularis (Wangemann, 1995), and as such, provide and maintain the high K^+ ionic environment within the vestibular labyrinth. It has previously been shown that the dark cells possess functional IsK channels at their apical membrane (Marcus and Shen, 1994). Thus, an examination was made of the dark cells at early postnatal ages, before extensive degeneration occurred in this region, in order to ascertain whether they undergo any degeneration in *isk* −/− mice. The best examples of dark cell degeneration were observed at P3 (Figures 8A and 8B). At this age, the cristae were still intact, but dark cells appeared to have undergone slight degeneration in *isk* −/− mice. Thus, while the dark cells in *isk* +/− mice (Figure 8A) had a crisp nuclear profile, presenting both hetero- and euchromatin, and cytoplasm apical to the nucleus, the dark cells of *isk* −/− mice contained a less well defined nuclear structure, and very little cytoplasm near the apical surface (Figure 8B). In addition, connective tissue was less abundant below the dark cell epithelium of *isk* −/− mice

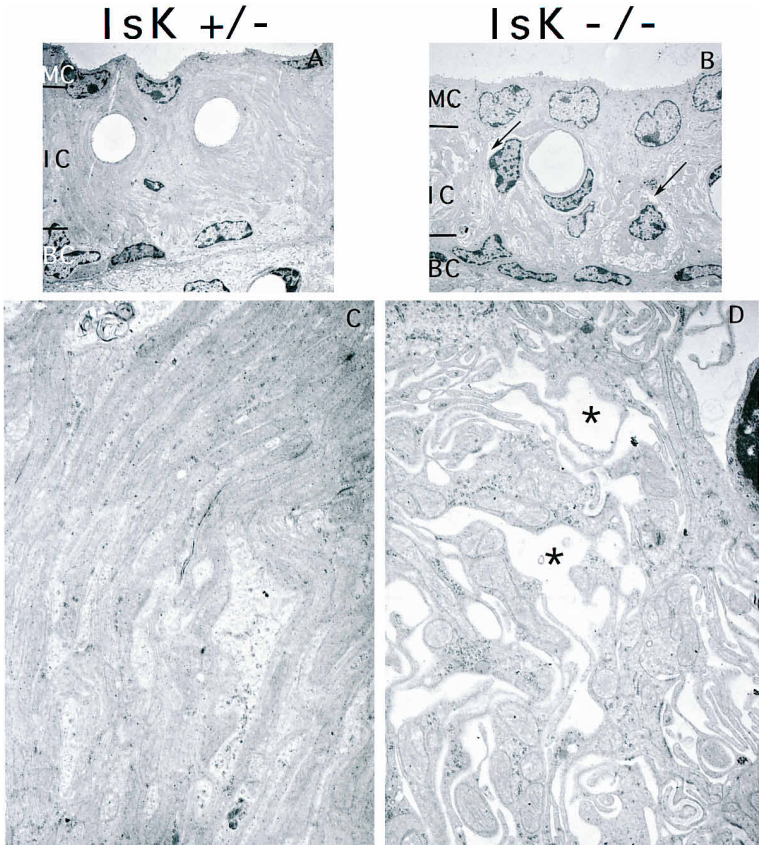

Figure 5. Electron Microscopy of the Stria Vascularis of *isk* +/− and *isk* −/− Mice

(A) The stria vascularis of *isk* +/− mice displays a smooth profile with no unusual characteristics. The marginal cell layer, intermediate cell layer, and basal cell layer can be discerned.

(B) The stria vascularis of *isk* −/− mice exhibits vacuoles within the intermediate cell layer (arrows). Additionally, some intermediate cells also appear vacuolated (lower right arrow). Basal and marginal cells appear grossly normal (original magnification for [A] and [B] 1.4 K).

(C) At high magnification, the interdigitation of cellular processes are smooth and orderly. Light processes originate from the intermediate cells, while the dark processes containing mitochondria eminate from the marginal cells.

(D) The same magnification of the intermediate cell layer of *isk* −/− mice illustrates the swollen intercellular spaces (asterisk). (Original magnification for [C] and [D] 10 K).

compared with either wild-type or *isk* +/− littermate controls. Finally, in terms of the dark cell epithelial sheet as a whole, *isk* −/− mice did not exhibit the typically smooth orderly apical membrane surface, but rather appeared jagged or scalloped (Figure 8B). However, no cell death was observed in the dark cell epithelial layer of the vestibular labyrinth.

Constitutive K^+ Secretion in Marginal Cells and Dark Cells

To demonstrate that the IsK channel is responsible for the K^+ current in strial marginal and vestibular dark cells, we measured the K^+ current in these cells in wild-type, *isk* +/−, and *isk* −/− mice. Strial marginal cells and vestibular dark cells were placed into a micro-Ussing chamber and both sides of the epithelium were perfused with a perilymph-like solution (NaCl solution, see Experimental Procedures). All samples of strial marginal cells and vestibular dark cells from wild-type mice or *isk* +/− mice developed a transepithelial voltage and thus a significant equivalent short circuit current (Figure 9). In contrast, none of the tissue samples from *isk* −/− mice was found to develop a transepithelial voltage exceeding the lower detection limit of ±0.5 mV. Transepi-

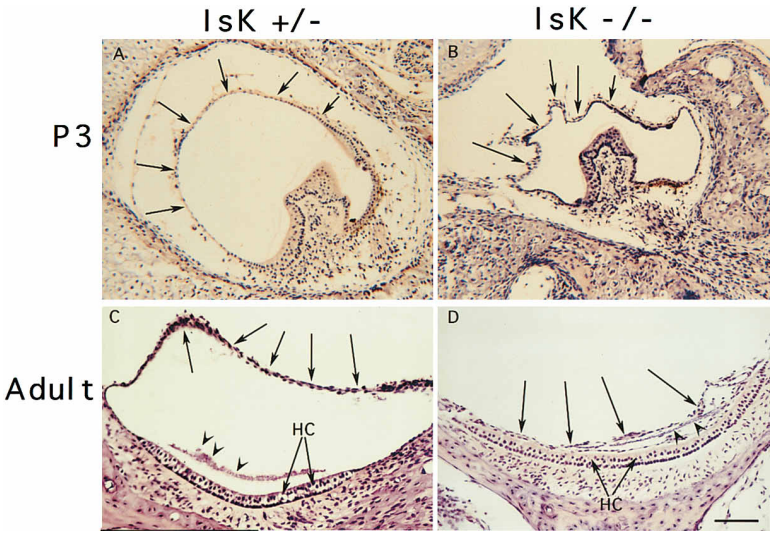

Figure 6. Position of the Vestibular Wall

(A) The vestibular wall surrounding the cristae in P3 *isk* +/− mice is fully and evenly distended (arrows).

(B) The vestibular wall surrounding the cristae in P3 *isk* −/− animals appears crenated and slightly collapsed in general (arrows).

(C) Similar to the situation in the cochlea, the vestibular wall (arrows) in *isk* +/− mice of all ages remained in its normal position, as shown here above the hair cells (HC) of the sacculus. Arrowheads point to otoconia.

(D) The collapse of the vestibular wall (arrows) was permanent in the *isk* −/− mice, as illustrated here above the macula sacculus (HC). Arrowheads point to otoconia. Note that the hair cells of the macula appear normal at this age (approximately 1 month old). Scale bar, 300 μm for (A) and (B); 100 μm for (C) and (D).

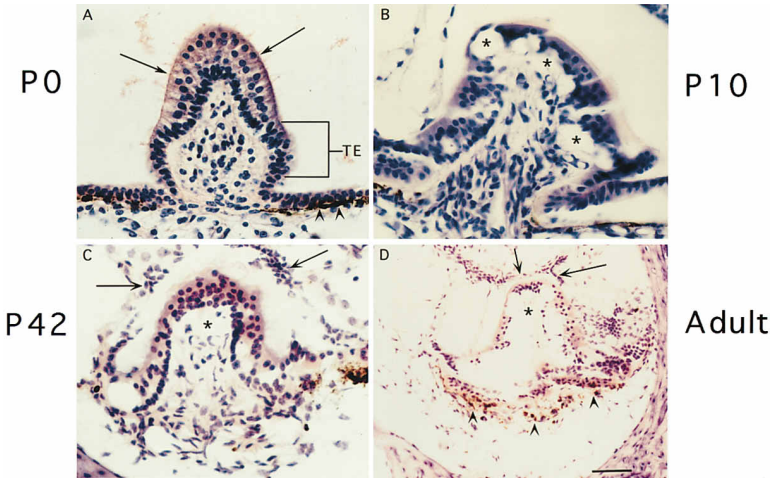

Figure 7. Hair Cell Death in the *isk* −/− Mouse Cristae

(A) At birth (P0), the cristae are already well developed. Hair cells are clearly identifiable (arrows) and the transitional epithelium (TE) is readily apparent. Below the TE is a row of melanocytes (arrowheads), above which lie the vestibular dark cells.

(B) The first signs of hair cell death in the cristae are seen at P10. Vacuoles have formed in the hair cell layer of the cristae (asterisk). However, many of the other structural components of the cristae can still be identified.

(C) By P42, the cristae have undergone massive degeneration. The core of the cristae, containing the nerve fibers coursing into the cristae to make contact with hair cells is severely vacuolated (asterisk). In addition, hair cells are difficult to identify.

(D) By 3 months of age, the cristae are only recognizable by the outline of dead or dying cells. The vestibular wall has collapsed completely down on what is left of the cristae (arrows) and the core is completely vacant of supporting cells and nerve fibers. Additionally, the dark cell epithelium and accompanying melanocytes are twisted and displaced under the cristae (arrowheads). Scale bar, 100 μm (A–C); 200 μm (D).

thelial resistances were significantly lower in tissues from mice lacking *isk* compared with the wild-type and *isk* +/− littermate controls. This lower transepithelial resistance was most likely due to altered mechanical properties of the tissue (see above and Figures 7 and 8), which limit the ability of the tissue to seal completely to the aperture of the micro-Ussing chamber. It is unlikely, however, that this lower resistance obscured a transepithelial voltage, since transepithelial voltages as high as 5 mV (>10-fold over noise) were measured in strial marginal cells at transepithelial resistances as small as 1 Ω-cm^2.

The rate of electrogenic K^+ secretion (J_K) was estimated from the equivalent short circuit current. J_K across strial marginal cells and vestibular dark cells of wild-type mice was 30 and 13 nmol $\times$ cm^{-2} $\times$ s^{-1}, respectively. J_K across strial marginal cells from *isk* +/− mice was 20 nmol $\times$ cm^{-2} $\times$ s^{-1}, which is significantly lower than in wild-type mice. There was, however, no significant difference between J_K across vestibular dark cells from *isk* +/− mice (9 nmol $\times$ cm^{-2} $\times$ s^{-1}) and from wild-type mice. J_K was close to zero in both strial marginal cells and vestibular dark cells of *isk* −/− mice, demonstrating that the J_K is mediated by the IsK channel.

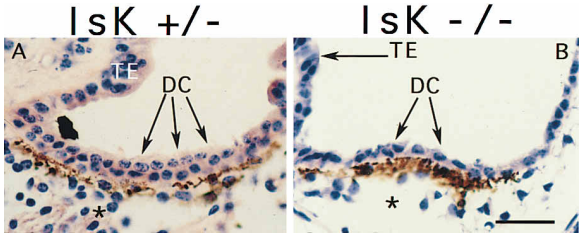

Figure 8. Vestibular Dark Cell Degeneration

(A) The vestibular dark cells, identified by their position above the melanocytes, appear normal in P3 *isk* +/− mice. Note the presence of connective tissue below the dark cell/melanocyte cell layer (asterisk). The vestibular dark cell epithelium appears smooth, and the nuclei of the cells are sharp and well differentiated with easily identifiable euchromatin and heterochromatin.

(B) The vestibular dark cells of P3 *isk* −/− mice do not appear normal. While the dark cells can still be identified by the association with the melanocytes, there is little connective tissue lying under the dark cell region. Additionally, the vestibular dark cell epithelium appears rough on the apical surface, and the morphology of the dark cell nuclei is not easily discerned. DC, vestibular dark cells; TE, transitional epithelium. Scale bar, 100 μm.

Regulation of K^+ Secretion in Dark Cells and Marginal Cells

Elevation of the basolateral K^+ concentration and apical perfusion of the IsK agonist DIDS (Shen et al., 1995) stimulate the rate of transepithelial K^+ secretion via stimulation of the IsK current. If the IsK current is necessary and sufficient for these increases in K^+ secretion, it would be expected that no stimulation of K^+ secretion would occur in epithelia from *isk* −/− mice.

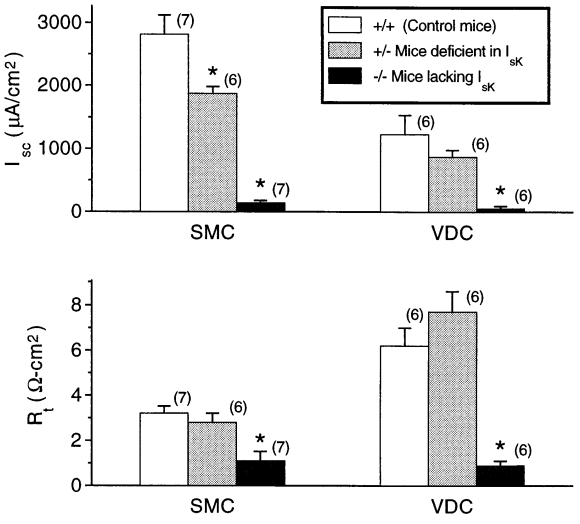

Figure 9. The Equivalent Short Circuit Current (I_{sc}) and the Transepithelial Resistance (R_t) of Strial Marginal Cells and Vestibular Dark Cells from Wild-Type Mice (+/+), *isk* +/− Mice, and *isk* −/− Mice

Significant differences toward data from control mice are marked (asterisk). The number of experiments is given in parentheses.

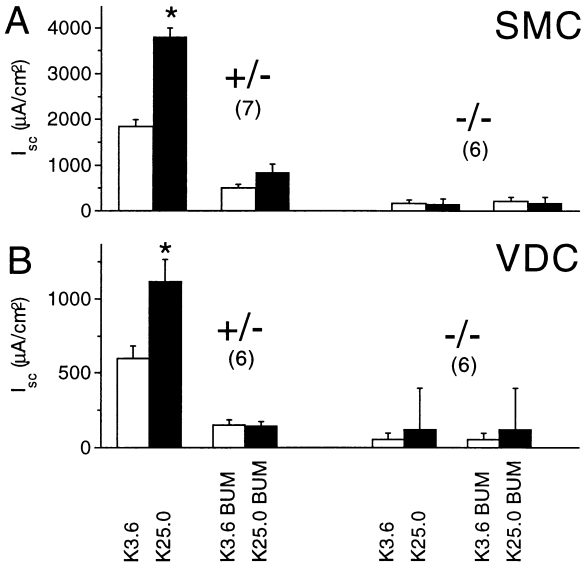

Figure 10. K^+-Induced Stimulation of the Equivalent Short Circuit Current (I_{sc}) across Strial Marginal Cells and Vestibular Dark Cells from *isk* +/− and *isk* −/− Mice

(A) Strial marginal cells.

(B) Vestibular dark cells.

The K^+ concentration in the basolateral perfusate was elevated from 3.6 to 25 mM (K3.6 and K25, respectively) in the absence and presence of 2×10^{-5} M bumetanide (BUM). Significant K^+-induced changes in I_{sc} are marked (asterisk). The number of experiments is given in parentheses.

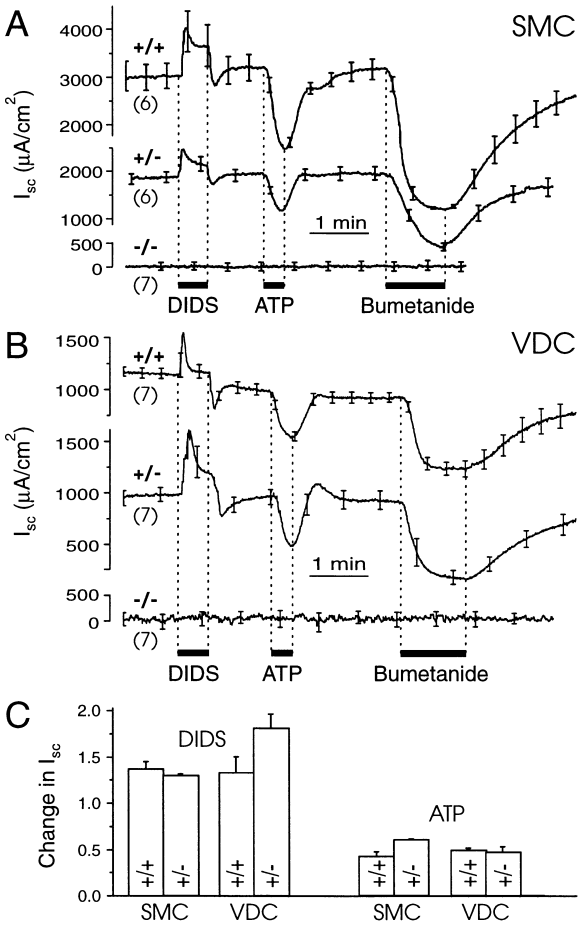

Figure 11. DIDS-Induced Stimulation and ATP- and Bumetanide-Induced Inhibition of the Equivalent Short Circuit Current (I_{sc}) across Strial Marginal Cells (SMC) and Vestibular Dark Cells (VDC) from Wild-Type (+/+), *isk* +/−, and *isk* −/− Mice

(A) Strial marginal cells.

(B) Vestibular dark cells.

(A)–(B) DIDS (1 mM) and 10^{-6} M ATP were applied to the apical perfusate. Bumetanide (2×10^{-5} M) was applied to the basolateral perfusate. Given is the average ± SEM, although for clarity not all error bars are shown. The number of experiments is given in parentheses.

(C) Comparison of the relative effects of DIDS and ATP in strial marginal cells (SMC) and vestibular dark cells (SMC). There were no significant differences among the responses to DIDS and to ATP.

An elevation of the basolateral K^+ concentration from 3.6 to 25 mM caused stimulation of K^+ secretion across strial marginal cells and vestibular dark cells from *isk* +/− mice (Figure 10). K^+-induced stimulation of K^+ secretion was absent in the presence of 2×10^{-5} M bumetanide in the basolateral perfusate (Figures 10 and 11). Thus, K^+ stimulation of K^+ secretion depends on the bumetanide-sensitive $Na^+/Cl^-/K^+$ cotransporter in the basolateral membrane of both epithelia (Wangemann and Marcus, 1990). However, K^+-stimulated K^+ secretion was absent in strial marginal cells and vestibular dark cells from *isk* −/− mice. These observations support the conclusion that the IsK current is essential not only for constitutive K^+ secretion, but also for K^+ stimulated K^+ secretion.

Addition of 1 mM DIDS to the apical perfusate of strial marginal cells and vestibular dark cells from wild-type mice and *isk* +/− mice caused an increase in the equivalent short circuit current consistent with an increase in the rate of K^+ secretion (Figure 11). DIDS-induced stimulation of K^+ secretion, however, was absent in strial marginal cells and vestibular dark cells from *isk* −/− mice, as expected if the IsK channel was not expressed. There was no significant difference in the relative increase of the equivalent short circuit current between epithelia from wild-type and *isk* +/− mice, or between strial marginal cells and vestibular dark cells. These observations suggest that IsK is essential for DIDS-stimulated K^+ secretion across both epithelia.

Application of 10^{-6} M ATP to the apical perfusate reversibly inhibited the equivalent short circuit current across strial marginal cells and vestibular dark cells from wild-type mice and *isk* +/− mice (Figure 11). This inhibition is thought to occur via second messenger cascades generated by activation of P_{2U} receptors located in the apical membranes of strial marginal cells and vestibular dark cells (Liu et al., 1995). There was no significant difference in the relative decrease of either the equivalent short circuit current across both epithelia between wild-type mice and *isk* +/− mice or between strial marginal cells and vestibular dark cells. Additionally, the equivalent short circuit current was also reversibly inhibited by 2×10^{-5} M bumetanide applied to the basolateral perfusate of strial marginal cells and vestibular dark cells from wild-type mice and *isk* +/− mice (Figure 11). It is

known that the bumetanide-sensitive $Na^+/Cl^-/K^+$ cotransporter is essential for the uptake of K^+ across the basolateral membrane of strial marginal cells and vestibular dark cells (Wangemann, 1995). Thus, K^+ secretion across both epithelia is sensitive to inhibition of the $Na^+/Cl^-/K^+$ cotransporter with bumetanide (Marcus et al., 1994; Marcus and Shipley, 1994; Wangemann et al., 1995a). Because there is no short circuit current observable in *isk* −/− mice, it was not possible to demonstrate its inhibition in the presence of either ATP or bumetanide.

Cell Volume Regulation in Dark Cells

Shrinking of vestibular dark cells following K^+-induced and osmotically induced cell swelling has been shown to involve activation of the IsK current in gerbils (Wangemann et al., 1995b; Wangemann et al., 1996). Thus, we hypothesized that vestibular dark cells from mice lacking *isk* would be unable to shrink if IsK would be essential for K^+ release during volume regulation. Vestibular dark cells were placed into a bath chamber on the stage of an inverted microscope equipped for the measurement of cell height. Cell swelling was either induced by an elevation in the K^+ concentration or by lowering the osmolarity in the basolateral perfusate.

Elevation of the extracellular K^+ concentration from 3.6 to 25 mM caused rapid cell swelling of vestibular dark cells from wild-type, *isk* +/−, and *isk* −/− mice (Figure 12). Cell height rose to a peak within 39–45 s, with no significant difference in the relative changes in cell height between the three different mouse genotypes. This K^+-induced cell swelling was completely blocked by 2×10^{-5} M bumetanide, a blocker of K^+ uptake via the $Na^+/Cl^-/K^+$ cotransporter. These observations suggest that the $Na^+/Cl^-/K^+$ cotransporter is present and functional in vestibular dark cells of all three mouse genotypes. Further, cell shrinking upon reduction of the K^+ concentration from 25 to 3.6 mM occurred in all three mouse genotypes within 2–3 min, suggesting that IsK, at least in mice, is not essential for volume regulation during K^+-induced cell swelling.

Lowering the osmolarity from 290 to 150 mosM caused rapid cell swelling of vestibular dark cells and subsequent regulatory volume decrease (Figure 12). No significant difference was observed in the initial osmotically induced cell volume increase or in the subsequent regulatory volume decrease between vestibular dark cells from *isk* +/− and *isk* −/− mice, suggesting that IsK, at least in mice, is also not essential for volume regulation after osmotically induced cell swelling.

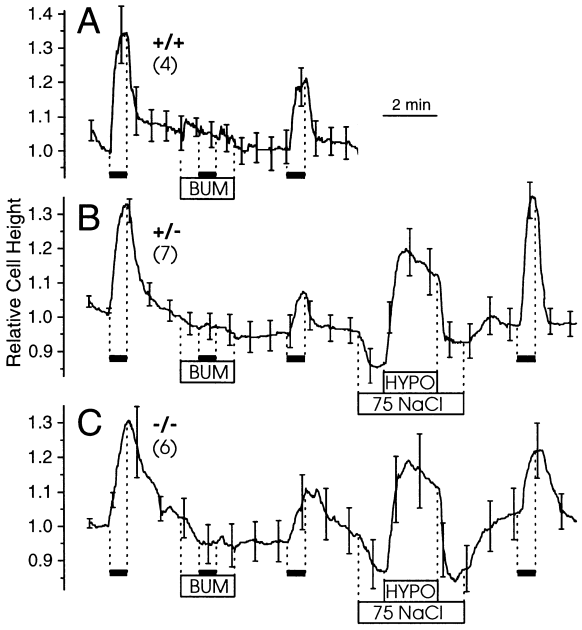

Figure 12. K^+-Induced Cell Swelling and Regulatory Volume Decrease of Vestibular Dark Cells from Wild-Type Mice (+/+), *isk* +/− Mice, and *isk* −/− Mice

(A) Wild-type mice (+/+).
(B) *isk* +/− mice.
(C) *isk* −/− mice.

The extracellular K^+ concentration was raised from 3.6 to 25 mM (filled bars) in the absence and presence of 2×10^{-5} M bumetanide (BUM). Regulatory volume decrease was observed in response to a hypo-osmotic challenge (HYPO), which was applied after the NaCl concentration had been reduced to 75 mM (75 NaCl). Average ± SEM of data expressed relative to the cell height before the first K^+ step, which was 6.0 ± 0.7 μm in wild-type mice, similar in *isk* +/− mice (6.9 ± 0.4 μm), and significantly larger (10.8 ± 1.3 μm) in *isk* −/− mice. For clarity, not all error bars are shown. The number of experiments is given in parentheses.

Discussion

The generation of mice carrying a null mutation on in the *isk* gene is described in this paper, along with behavioral, anatomical, and physiological analyses of these mice. Null mutation of the *isk* gene involved a complete deletion of the coding region for IsK. Behaviorally, *isk* −/− mice exhibited hyperactivity, bidirectional circling, head tilt, and head bobbing. Such behavior has been classically described in mutant mice of the Shaker and Waltzer families (Deol, 1956, 1954; Lyon et al., 1996), and the behavior has therefore been referred to as a shaker/waltzer phenotype. The shaker/waltzer behavior has long been recognized as being indicative of inner ear dysfunction (Deol, 1956, 1954). However, such behavior can occur with wide ranging severity of inner ear abnormalities (Lyon et al., 1996).

Swimming behavior can be used to diagnose the severity of inner ear dysfunction (Sawada et al., 1994). Indeed, a number of different swimming postures have been described for mice with various states of inner ear abnormalities (Lim et al., 1978), and generally have been linked to the anatomical and functional state of the otolith organs. While anatomically the otolith organs of *isk* +/− and *isk* −/− mice did not appear to be undergoing any degenerative changes at the ages the animals were tested, *isk* −/− mice nonetheless could not swim. The most likely explanation for this is that the vestibular labyrinth does not contain its normal endolymph composition and volume, and thus, even though cells of the otolith organs appeared structurally normal (as assessed by light microscopy) at the time of the swim test, normal transduction could not occur. In addition, the collapse of the vestibular wall onto the otoconia probably hindered their movement. The final result would be

to cause the animals to lose orientation with respect to gravity when tactile cues (such as feet touching the bottom of the cage) are removed.

The timing of the collapse of Reissner's membrane in *isk* −/− mice correlates well with what is known about the maturation of strial cells and the generation of the K^+ concentration within scala media of neonatal mice. The collapse occurred at P3, paralleling the time when the great majority of strial cells have become postmitotic (Ruben, 1967). X-ray energy dispersive techniques (Anniko and Nordemar, 1980; Anniko and Wroblewski, 1981) have shown that the rise toward a mature endolymphatic K^+ concentration begins between P2 and P4, indicating that IsK channels are normally functioning at this time, and further that the tight junctions between strial marginal cells have sufficiently matured to allow an isolated ionic environment to develop and be maintained in scala media. Thus, it can be assumed that little, if any, volume can be added to the endolymphatic space without K^+ going through the IsK channels once the apical membranes of the strial marginal cells express their tight junctions. Without functioning IsK channels, the volume of endolymph would not increase significantly. Assuming that the normal ion reabsorptive pathways within the organ of Corti remain functional, the endolymphatic space might actually be under negative pressure. The end result would be that the endolymphatic space would lose volume and pressure, allowing the normal perilymphatic pressure from scala vestibuli to distort Reissner's membrane and push it toward the lateral wall of the cochlea. While not illustrated in the results, it should be noted that the endolymphatic duct and sac did not show signs of a change in volume in *isk* −/− mice.

The *isk* −/− mice exhibited degeneration of hair cells in the inner ear. The timing of when any specific hair cell degenerated seemed closely correlated with the organ to which that hair cell belonged. Thus, hair cells of the organ of Corti died very early, while hair cells of the cristae ampullaris died approximately 1 week later, and, finally, hair cells of the saccular maculae died many months later. Therefore, two questions are raised: why do hair cells die and why do hair cells of different organs die at different times?

Plausible explanations for hair cell death are certain to be complex, and probably involve the transduction channels and/or other apically located transporters in hair cells, the populations of different channels and ion exchangers in the basolateral membrane of these cells, and the presumably abnormal composition of the endolymph in the *isk* −/− mice. In brief, hair cell death may be attributable to calcium toxicity. Given that the permeability of the transduction channels for calcium is four times higher than that for K^+ in isolated chick hair cells (Ohmori, 1985), the predominant ion fluxed through the transduction channel in the absence of potassium is likely to be calcium. A higher cytosolic calcium level has been suggested to lead to a slowing of its further diffusion within the cell, thereby also slowing the termination of K^+ channel activity (Hudspeth and Lewis, 1988) following spontaneous activity, allowing internal K^+ concentrations to decline and voltage gated calcium channels to remain open longer, thus further increasing the internal calcium concentrations.

The actual time of hair cell degeneration depended on the particular inner ear organ containing the hair cells, but different hair cell types within each organ degenerated at the same time. For example, both inner and outer hair cells of the organ of Corti degenerated approximately at P3, while the Type I and Type II hair cells of the cristae degenerated at about P10. It has been shown that 1) different receptor organs in the same animal, 2) different hair cell types within the same receptor organ, and 3) the same receptors in different species express different hair cell active and passive membrane properties, collectively known as filtering properties (Correia, 1992). Each hair cell requires a specific repertoire of ion channels to facilitate filtering of the transduction event in their particular frequency range in order to augment any response at a critical frequency or over a range of frequencies (Correia, 1992). With different filtering properties, each hair cell type is likely to be differentially susceptible to the above mentioned mechanisms of cell death.

An explanation can also be proposed for understanding why the otolith organ hair cells survive so much longer than other hair cell types. The saccule and utricle are different from other inner ear structures in that they possess otoconia, calcium-rich crystals that lie over the hair cell regions (the maculae) in each of these areas. It has been shown previously that the maculae in each of the otolith organs produce and exude the large quantities of calcium needed for the formation of otoconia (Anniko, 1980). Therefore, these structures, which include the hair cells, have faced locally high calcium concentrations, and may express unusual buffering mechanisms that help the cells survive through changes in endolymphatic ion composition. Thus, these cells may have a wider homeostatic range within which they can survive and function.

Spiral ganglion cell death occurs in *isk* −/− mice, and presumbly represents a secondary degenerative effect to the lack of *isk* gene expression, since IsK is not expressed by these cells. Ganglion cells in older animals survive relatively well without support from their targets, as exemplified by ototoxically deafened animals, and the relatively rare occurences of cell death can be at least partially blocked by delivering electrical stimulation to an ear devoid of hair cells (Leake and Hradek, 1988; Leake et al., 1991, 1992). Thus, ganglion cell death in these cases may be explained by a lack of activity rather than an absence of targets. A mechanistic explanation for why there is decreased cell death at the apical regions of the cochlea compared with the base and middle turns remains elusive.

Previous studies in gerbils suggested that IsK is essential for constitutive and stimulated K^+ secretion across strial marginal cells and vestibular dark cells (Marcus and Shen, 1994; Shen et al., 1996; Wangemann et al., 1995a). The present study definitively demonstrates this function in mouse from a genetic perspective. Short circuit current measurements indicated a high rate of K^+ secretion in wild-type and *isk* +/− mice, while no significant current could be detected in *isk* −/− mice even under conditions shown to stimulate IsK channel activity. In contrast, cell volume regulation was preserved in vestibular dark cells from *isk* −/− mice, indicating that IsK is not essential for this function. Moreover, the fact that cell swelling is sensitive to bumetanide

in *isk* −/− mice indicates that the $Na^+/Cl^-/K^+$ cotransporter is not down-regulated. Given that the $Na^+/Cl^-/K^+$ cotransporter is functional in *isk* −/− mice, and that volume regulation is not compromised, one must rule out the possibility of a lack of K^+ flux across the apical membrane owing to impairment of K^+ entry into the cell.

The *isk* knockout–induced deafness syndrome in mice shares some similarity with other known mouse and human models of deafness, but when details are considered, seems to represent a new model of deafness. All known human classes of deafness have been described in mutant mice (Deol, 1968; Steel and Bock, 1983). The most frequently encountered class of deafness observed in humans is the Scheibe type deafness (Deol, 1968), the cochlear pathology of which resembles that exhibited by *isk* −/− mice, with a collapse of Reissner's membrane and a degeneration of the organ of Corti. The Scheibe type deafness is also known as a cochleosaccular deafness, since both the cochlea and saccular macula degenerate. However, there is no involvement of either the utricle or cristae in Scheibe type deafness (Deol, 1968). Additionally, upon closer examination, Scheibe type deafness was determined to be of a morphogenetic variety, with indications of a poorly developed stria vascularis and faulty final stages of differentiation of the cochlea and saccule (Deol, 1963). However, for a number of reasons, *isk* knockout–induced deafness may represent a new class of deafness. While the degenerative end point of *isk* gene ablation results in a similar cochleosaccular pathology to Scheibe type deafness, degeneration is not limited to this region. Also, the *isk* knockout–induced deafness cannot be classified as morphogenetic given that initially the inner ear develops normally.

A pathology strikingly similar to that observed in *isk* −/− mice was reported upon post-mortem inspection of the inner ears of patients clinically diagnosed with a "cardioauditory" syndrome (Friedmann et al., 1968, 1966) known as Jervell and Lange-Nielsen syndrome (Cusimano et al., 1991; Fraser et al., 1964; Friedmann et al., 1966; Jervell and Lange-Nielsen, 1957). Patients suffering from Jervell and Lange-Nielsen syndrome exhibit a prolonged Q-T wave interval and profound deafness from birth. However, genes thus far described as involved in long Q-T wave syndromes (Curran et al., 1995; Sanguinetti et al., 1995) seem not to be involved in auditory function or development. Preliminary experiments (Tesson et al., 1996) did not find evidence to support the hypothesis that Jervell and Lange-Nielsen syndrome is caused by a defect in the *isk* gene, although further work must be done to definitively rule out *isk* as being causally involved in this particular disease. Candidate genes for this and other probable cardioauditory syndromes (Koroxenidis et al., 1966; Lewis et al., 1958) have yet to be described.

Finally, in light of the recent reports (Barhanin et al., 1996; Sanguinetti et al., 1996) showing that IsK coassembles with KvLQT1 and that IsK expressed in the absence of KvLQT1 in CHO cells does not yield a functional K^+ channel, it will be of interest to examine whether the marginal cells of the stria vascularis and/or the vestibular dark cells express KvLQT1. In the absence of KvLQT1 expression in the inner ear, it would then be necessary to postulate that IsK can coassemble with other, as yet uncharacterized, K^+ channel subunits.

Experimental Procedures

Targeting Vector Construction and Generation of *isk*-Deficient Mice

The mouse *isk* gene was isolated from a mouse genomic library prepared from 129/Sv mice DNA (kindly provided by Dr. Bernhard Bettler, Ciba [Novartis]). A clone with an insert of 18 kb was characterized as containing the entire exon 2, flanked by 9 kb 5′ and 7 kb 3′ intronic sequences. The targeting vector consisted of an 8.1 kb EcoR1 restriction fragment that was subcloned into pBluescript (Stratagene) and in which the 1.2 kb BamHI–SphI fragment containing the entire coding region was replaced by the 1.6 kb neomycin resistance gene under the control of the PGK promoter. The herpes simplex thymidine kinase gene placed under the control of the MC1 promoter was added to the 5′ end of the mouse DNA and the vector was linearized on the opposite edge before electroporation into ES cells.

Methods for cell culture and transfection were essentially as described previously (Köntgen and Stewart, 1993; Stewart, 1993). In brief, 129/Sv ES cells of the W9.5 line (Szabo and Mann, 1994) were electroporated in the presence of the targeting vector (1×10^7 cells and 25 mcg DNA) four times, and plated onto mitomycin C–inactivated STO mouse transformed fibroblast cells transfected with the bacterial neomycin and human LIF genes (kindly supplied by Frank Conlon and Liz Robertson). Cells were subjected to Geneticin (GIBCO/BRL, 175 mcg/ml active weight) and Cytovene (ganciclovir, Syntex Laboratories Inc., 2 mcM) selection. Of 145 clones, 5 were homologous recombinants. These clones were expanded without selection and two were injected into C57BL/6J blastocysts. Chimeras from one clone were mated with 129/Sv females, and germ line transmission confirmed first by glucose phosphate isomerase-1 isozyme analysis (Hogan et al., 1994), then by analysis for the mutation. The mutation has been maintained on the 129/Sv background by breeding *isk* −/+ females (no overt phenotype) with *isk* −/− males. Primers to *isk* (5′CCAGGATGAGCCTGCCCAAT3′ and 5′AGGAAGG TGTGTG GCAG3′) were used to amplify a 373 bp *isk* cDNA by RT–PCR in mRNA isolated from heart, kidney, and submandibular glands from wild-type and *isk* −/− animals. The PCR products were resolved on agarose gel, blotted onto nylon, and revealed by hybridization with an *isk* ^{32}P-labeled cDNA fragment.

Swimming Behavior Analysis

Mice, approximately 3 weeks old, were tested for their swimming ability. In all, three groups (wild type, *isk* +/−, and *isk* −/−) of five mice each were tested. A small tank was filled to a depth of approximately 9 inches with ambient temperature water. Mice were carefully lowered into the water by hand only after all apparent agitation (as judged visually) had subsided. Mice were allowed to swim continuously for 30 s per trial, and each mouse was subjected to a swimming trial once. The swimming posture of each animal was observed and grossly scored according to the degree to which the animal deviated from the horizontal plane while swimming (data not shown).

Histology

Animals used for this study were aged E17.5, P0, P3, P7, P10, P20, P42, 3 months, 5 months, and 7 months old (E0.5 being defined as the day a vaginal plug was discovered, and P0 being defined as the day of birth). All animals were transcardially perfused with 4% paraformaldehyde in 0.1 M sodium phosphate buffer (pH 7.2–7.4), the temporal bones were isolated and postfixed overnight and then decalcified in 8% EDTA and 4% paraformaldehyde in phosphate buffered saline. Finally, the temporal bones were dehydrated and embedded either in paraffin following routine procedures, or in LR White resin following instructions included with the product. Paraffin sections were cut between 5 and 12 μm thick, while plastic sections were cut at 4 μm thick. All sections were saved and mounted onto glass slides and counterstained with either hematoxylin and eosin (paraffin sections) or toluidine blue (plastic sections).

Electron Microscopy

One *isk* +/− and one *isk* −/− animal approximately 1 month old were selected for EM analysis of the stria vascularis. Animals were transcardially perfused first with warm phosphate buffered saline

vascular rinse (pH 7.2), followed by a fixative comprised of 2.5% glutaraldehyde and 2% paraformaldehyde in 0.13 M sodium phosphate buffer (ph 7.3). Following the perfusion, the temporal bones were isolated and post-fixed overnight at 4°C. Decalcification was done in a solution containing 2.5% glutaraldehyde, 2% paraformaldehyde, 0.12 M sodium phosphate buffer, and 6.4% EDTA for 1 week, after which the tissues were stained en bloc with uranyl acetate, osmicated, and routinely processed for electron microscopy. Grey to silver sections were cut and examined in a JEOL 100CX electron microscope.

Cell Profile Counting and Statistical Analysis

Spiral ganglion cell profiles from P7, P20, P42, and 7-month-old animals were counted in plastic embedded sections. Three 4 μm thick mid-modiolar sections were used for obtaining a count in each turn of the cochlea, and these sections were matched with other animals in the same age group. Thus, the same level of the cochlea was used for examination between animals of the same age. Because of the thickness of the section (4 μm) and the spacing between the sections used for counting (24 μm), each cellular profile represented a unique cell body profile. However, it must be cautioned that counts between age groups may not be reliably compared, as no control was exercised in matching these sections with others of different age groups, owing to the fact that the cochlea was still undergoing postnatal maturation at some of the ages examined. A paired t-test was employed, and the results graphed, using the StatView computer program. Data are given as average ± 1 standard deviation. Significance was assumed when $P < 0.05$.

Equivalent Short Circuit Current

The equivalent short circuit current was obtained as described earlier (Marcus et al., 1994). In brief, the epithelium was sealed with the apical membrane onto the aperture of the micro-Ussing chamber. The transepithelial voltage and resistance were measured with calomel electrodes connected to the chamber via agar bridges made with NaCl solution (see below). Transepithelial current pulses were passed via Ag/AgCl wires. Sample-and-hold circuitry was used to obtain a signal proportional to the transepithelial resistance from the voltage response to the current pulses (50 nA for 34 ms at 0.3 Hz). In parallel, the data were digitized omitting, for clarity, the responses to the current pulses. When the K^+ concentration was raised from 3.6 to 25 mM, the transepithelial voltage was corrected for a liquid junction potential of 0.5 mV. The transepithelial resistance was normalized for the area defined by the aperture of the micro-Ussing chamber (diameter of aperture: 80 μm). Solution changes in the apical and basolateral perfusate were complete within 1 s. The equivalent short circuit current was calculated from measurements of the transepithelial voltage and resistance according to Ohm's law (equivalent short circuit current = transepithelial voltage/transepithelial resistance). The rate of K^+ secretion (J_K) was estimated from the equivalent short circuit current according to J_K = equivalent short circuit current/F, where F is the Faraday constant (9.45×10^4 $A \times s \times mol^{-1}$) (Marcus and Marcus, 1987; Wangemann et al., 1996).

Cell Height

Cell height was measured as previously described (Wangemann and Shiga, 1994). In brief, the microscope image of the folded tissue was viewed with a black/white video camera (Panasonic WV-1550), mixed with a time signal, and displayed on a monitor (PVM-122, Sony, Park Ridge, NJ) as well as recorded on videotape (AG-1960, Panasonic, Secaucus, NJ). A computer-generated image of two vertical cursors was mixed on-line with the microscope image (Televeyes, Digital Inc., Dedham, MA). The two cursors were adjusted independently to overlay the apical and basal border of the vestibular dark cell epithelium. The calibrated distance between the two cursors (cell height) was written into an ASCII file at a rate of 0.5 Hz. Analysis of the ASCII files was performed in a programmable data analysis program (Origin 3.78, Microcal Software, Northampton, MA). Data were normalized to the cell height before the first elevation of the K^+ concentration.

Solutions Used for Physiological Experiments

NaCl solution contained (in mM): 150 NaCl, 1.6 K_2HPO_4, 0.4 KH_2PO_4, 0.7 $CaCl_2$, 1.0 $MgCl_2$, and 5.0 glucose. The K^+ concentration was elevated from 3.6 to 25 mM by isosmotic replacement of 21.4 mM NaCl from KCl. Prior to a hypo-osmotic challenge, the 75 mM NaCl was replaced with 150 mM mannitol. The hypo-osmotic challenge consisted of removal of 150 mM mannitol, which reduced the osmolarity from about 290 to about 150 mosM. All solutions were titrated to pH 7.4.

Animal Handling

All animals used in experiments reported here were housed and handled under protocols approved by the Institutional Animal Care and Use Committees at the respective institutions involved.

Acknowledgments

Correspondence should be addressed to D. E. V. or J. B. This work was supported by the Centre de la Recherche Scientifique (CNRS) the Ministère de l'Enseignement Superieur et de la Recherche, MESR ACC N° 9509 113 and the Association Francaise contre les Myopathies (AFM) (J. B.); NIH grants NS 28709, NS 11549, and DC 02871 (S. F. H.); and DC 01098 (P. W.).

The costs of publication of this article were defrayed in part by the payment of page charges. This article must therefore be hereby marked *"advertisement"* in accordance with 18 USC Section 1734 solely to indicate this fact.

Received October 8, 1996; revised November 6, 1996.

References

Anniko, M. (1980). Development of otoconia. Am. J. Otolaryngol. *1*, 400–410.

Anniko, M., and Nordemar, H. (1980). Embryogenesis of the inner ear. IV. Post-natal maturation of the secretory epithelia of the inner ear in correlation with the elemental composition in the endolymphatic space. Arch. Otorhinolaryngol. *229*, 281–288.

Anniko, M., and Wroblewski, R. (1981). Elemental composition of the developing inner ear. Ann. Otol. Rhinol. Laryngol. *90*, 25–32.

Attali, B., Romey, G., Honore, E., Schmid-Alliana, A., Mattei, M.G., Lesage, F., Ricard, P., Barhanin, J., and Lazdunski, M. (1992). Cloning, functional expression, and regulation of two K+ channels in human T lymphocytes. J. Biol. Chem. *267*, 8650–8657.

Barhanin, J., Lesage, F., Guillemare, E., Fink, M., Lazdunski, M., and Romey, G. (1996). KVLQT1 and IsK (minK) proteins associate to form the Iks cardiac potassium current. Nature *382*, 78–80.

Belal, A., and Ylikoski, J. (1980). Pathologic significance of Meniere's symptom complex: a histopathologic and electron microscopic study. Am. J. Otolaryngol. *1*, 275–284.

Bezanilla, F., Perozo, E., and Stefani, E. (1994). Gating of Shaker K+ channels. II. The components of gating currents and a model of channel activation. Biophys. J. *66*, 1011–1021.

Busch, A.E., Malloy, K., Groh, W.J., Varnum, M.D., Adelman, J.P., and Maylie, J. (1994). The novel class III antiarrhythmics NE-10064 and NE-10133 inhibit IsK channels expressed in Xenopus oocytes and IKs in guinea pig cardiac myocytes. Biochem. Biophys. Res. Commun. *202*, 265–270.

Busch, A.E., Suessbrich, H., Waldegger, S., Greger, R., Lang, H.J., Lang, F., Gibson, J.K., and Maylie, J. (1996). Inhibition of IKs in guinea pig cardiac myocytes and guinea pig IsK channels by chromanol 293B. Plugers Arch., in press.

Correia, M.J. (1992). Filtering properties of hair cells. Ann. NY Acad. Sci. *656*, 49–57.

Curran, M.E., Splawski, I., Timothy, K.W., Vincent, G.M., Green, E.D., and Keating, M.T. (1995). A molecular basis for cardiac arrhythmia: HERG mutations cause long QT syndrome. Cell *80*, 795–803.

Cusimano, F., Martines, E., and Rizzo, C. (1991). The Jervell and Lange-Nielsen syndrome. Int. J. Pediatr. Otorhinolaryngol. *22*, 49–58.

Deol, M.S. (1954). The anomalies of the labyrinth of the mutants varitint-waddler, shaker-2, and jerker in the mouse. J. Genet. *52*, 562–588.

Deol, M.S. (1956). The anatomy and development of the mutants pirouette, shaker-1, and waltzer in the mouse. Proc. R. Soc. Lond. (Biol.) *145*, 206–213.

Deol, M.S. (1963). The development of the inner ear in mice homozygous for shaker-with-syndactylism. J. Embryol. Exp. Morphol. *4*, 493–512.

Deol, M.S. (1968). Inherited diseases of the inner ear in man in light of studies on the mouse. J. Mol. Gen. *5*, 137–158.

Doupnik, C.A., Davidson, N., and Lester, H.A. (1995). The inward rectifier potassium channel family. Curr. Opin. Neurobiol. *5*, 268–277.

Felipe, A., Knittle, T.J., Doyle, K.L., Snyders, D.J., and Tamkun, M.M. (1994). Differential expression of Isk mRNAs in mouse tissue during development and pregnancy. Am. J. Physiol. *267*, C700–705.

Folander, K., Smith, J.S., Antanavage, J., Bennett, C., Stein, R.B., and Swanson, R. (1990). Cloning and expression of the delayed-rectifier IsK channel from neonatal rat heart and diethylstilbestrol-primed rat uterus. Proc. Natl. Acad. Sci. USA *87*, 2975–2979.

Fraser, G.R., Froggatt, P., and Murphy, T. (1964). Genetical aspects of the cardio-auditory syndrom of Jervell and Lange-Nielsen (congenital deafness and electrocardiographic abnormalities). Ann. Hum. Gen. Lond. *28*, 133–157.

Freeman, L.C., and Kass, R.S. (1993). Delayed rectifier potassium channels in ventricle and sinoatrial node of the guinea pig: molecular and regulatory properties. Cardiovasc. Drugs Ther. *7*, 627–635.

Friedmann, I., Fraser, G.R., and Froggatt, P. (1966). Pathology of the ear in the cardioauditory syndrome of Jervell and Lange-Nielsen (recessive deafness with electrocardiographic abnormalities). J. Laryngol. Otol. *80*, 451–470.

Friedmann, I., Fraser, G.R., and Froggatt, P. (1968). Pathology of the ear in the cardio-auditory syndrome of Jervell and Lange-Nielsen. Report of a third case with an appendix on possible linkage with the Rh blood group locus. J. Laryngol. Otol. *82*, 883–896.

Heginbotham, L., Lu, Z., Abramson, T., and MacKinnon, R. (1994). Mutations in the K+ channel signature sequence. Biophys. J. *66*, 1061–1067.

Hinojosa, R., and Rodriguez-Echandia, E.L. (1966). The fine structure of the stria vascularis of the cat inner ear. Am. J. Anat. *118*, 631–664.

Hogan, B., Beddington, R., Costantini, F., and Lacy, E. (1994). Manipulating the Mouse Embryo: A Laboratory Manual (Cold Spring Harbor, New York: Cold Spring Harbor Press).

Honore, E., Attali, B., Romey, G., Heurteaux, C., Ricard, P., Lesage, F., Lazdunski, M., and Barhanin, J. (1991). Cloning, expression, pharmacology and regulation of a delayed rectifier K+ channel in mouse heart. EMBO J. *10*, 2805–2811.

Hudspeth, A.J., and Lewis, R.S. (1988). Kinetic analysis of voltage and ion-dependent conductances in saccular hair cells of the bull frog, Rana catesbeiana. J. Physiol. (Lond.) *400*, 237–274.

Jan, L.Y., and Jan, Y.N. (1994). Potassium channels and their evolving gates. Nature *371*, 119–122.

Jervell, A., and Lange-Nielsen, F. (1957). Congenital deaf-mutism, functional heart disease with prolongation of the Q-T interval, and sudden death. Am. Heart J. *54*, 59–68.

Köntgen, F., and Stewart, C.L. (1993). Simple screening procedure to detect gene targeting events in embryonic stem cells. Meth. Enzymol. *225*, 878–890.

Koroxenidis, G.T., Webb, N.C., Moschos, C.B., and Lehan, P.H. (1966). Congenital heart disease, deaf-mutism and associated somatic malformations occuring in several members of one family. Am. J. Med. *40*, 149–155.

Leake, P.A., and Hradek, G.T. (1988). Cochlear pathology of long term neomycin induced deafness in cats. Hearing Res. *33*, 11–33.

Leake, P.A., Hradek, G.T., Rebscher, S.J., and Snyder, R.L. (1991). Chronic intracochlear electrical stimulation induces selective survival of spiral ganglion neurons in neonatally deafened cats. Hearing Res. *54*, 251–271.

Leake, P.A., Snyder, R.L., Hradek, G.T., and Rebscher, S.J. (1992). Chronic intracochlear electrical stimulation in neonatally deafened cats: effects of intensity and stimulating electrode location. Hearing Res. *64*, 99–117.

Lesage, F., Attali, B., Lazdunski, M., and Barhanin, J. (1992). ISK, a slowly activating voltage-sensitive K+ channel. Characterization of multiple cDNAs and gene organization in the mouse. FEBS Lett. *301*, 168–172.

Lesage, F., Guillemare, E., Fink, M., Duprat, F., Lazdunski, M., Romey, G., and Barhanin, J. (1996). Twik-1, a ubiquitous human weakly inward rectifying K+ channel with a novel structure. EMBO J. *15*, 1004–1011.

Lewis, S.M., Sonnenblick, B.P., Gilbert, L., and Biber, D. (1958). Familial pulmonary stenosis and deaf-mutism: clinical and genetic considerations. Am. Heart J. *55*, 458–462.

Li, M., Unwin, N., Stauffer, K.A., Jan, Y.N., and Jan, L.Y. (1994). Images of purified Shaker potassium channels. Curr. Biol. *4*, 110–115.

Lim, D.J., Erway, L.C., and Clark, D.L. (1978). Tilted-head mice with genetic otoconial anomaly. Behavioral and morphological correlates. In Vestibular Mechanisms in Health and Disease, J.D. Hood, ed. (New York: Academic Press), pp. 195–206.

Liu, J., Kozakura, K., and Marcus, D.C. (1995). Evidence for purinergic receptors in vestibular dark cell and strial marginal cell epithelia of the gerbil. Audit. Neurosci. *1*, 331–340.

Logothetis, D.E., Movahedi, S., Satler, C., Lindpaintner, K., and Nadal-Ginard, B. (1992). Incremental reductions of positive charge within the S4 region of a voltage-gated K+ channel result in corresponding decreases in gating charge. Neuron *8*, 531–540.

Lyon, M., Rastan, S., and Brown, S.D.M. (1996). Genetic Variants and Strains of the Laboratory Mouse (New York: Oxford Press).

MacKinnon, R. (1995). Pore loops: an emerging theme in ion channel structure. Neuron *14*, 889–892.

Marcus, N.Y., and Marcus, D.C. (1987). Potassium secretion by nonsensory region of gerbil utricle in vitro. Am. J. Physiol. *253*, F613–621.

Marcus, D.C., and Shen, Z. (1994). Slowly activating voltage-dependent K+ conductance is apical pathway for K+ secretion in vestibular dark cells. Am. J. Physiol. *267*, C857–864.

Marcus, D.C., and Shipley, A.M. (1994). Potassium secretion by vestibular dark cell epithelium demonstrated by vibrating probe. Biophys. J. *66*, 1939–1942.

Marcus, D.C., Liu, J., and Wangemann, P. (1994). Transepithelial voltage and resistance of vestibular dark cell epithelium from the gerbil ampulla. Hearing Res. *73*, 101–108.

Ohmori, H. (1985). Mechano-electrical transduction current in isolated vestibular hair cells of the chick. J. Physiol. *359*, 189–217.

Pascual, J.M., Shieh, C.C., Kirsch, G.E., and Brown, A.M. (1995). K+ pore structure revealed by reporter cysteines at inner and outer surfaces. Neuron *14*, 1055–1063.

Pongs, O. (1992). Molecular biology of voltage-dependent potassium channels. Physiol. Rev. *72*, S69–88.

Pongs, O. (1993). Structure-function studies on the pore of potassium channels. J. Membr. Biol. *136*, 1–8.

Ruben, R.J. (1967). Development of the inner ear of the mouse: a radioautographic study of terminal mitoses. Acta Otolaryngol. Suppl. (Stockh.) *220*, 1–44.

Sakagami, M., Fukazawa, K., Matsunaga, T., Fujita, H., Mori, N., Takumi, T., Ohkubo, H., and Nakanishi, S. (1991). Cellular localization of rat Isk protein in the stria vascularis by immunohistochemical observation. Hearing Res. *56*, 168–172.

Sanguinetti, M.C., Jiang, C., Curran, M.E., and Keating, M.T. (1995). A mechanistic link between an inherited and an acquired cardiac arrhythmia: HERG encodes the IKr potassium channel. Cell *81*, 299–307.

Sanguinetti, M.C., Curran, M.E., Zou, A., Shen, J., Spector, P.S., Atkinson, D.L., and Keating, M.T. (1996). Coassembly of KVLQT1 and mink (IsK) proteins to form cardiac Iks potassium channel. Nature *382*, 80–83.

Sawada, I., Kitahara, M., and Yazawa, Y. (1994). Swimming test

for evaluating vestibular function in guinea pigs. Acta Otolaryngol. Suppl. (Stockh.) *510*, 20–23.

Shen, Z., Liu, J., Marcus, D.C., Shiga, N., and Wangemann, P. (1995). DIDS increases K+ secretion through an IsK channel in apical membrane of vestibular dark cell epithelium of gerbil. J. Membr. Biol. *146*, 283–291.

Shen, Z., Marcus, D.C., Shiga, N., and Wangemann, P. (1996). IsK channel in strial marginal cell: voltage-dependance, ion selectivity, inhibition by 293B and sensitivity to clofilium. Audit. Neurosci., in press.

Sher, A.E. (1971). The embryonic and postnatal development of the inner ear of the mouse. Acta Otolaryngol. Suppl. (Stockh.) *285*, 1–77.

Steel, K.P., and Bock, G.R. (1983). Hereditary inner ear abnormalities in animals. Arch. Otolaryngol. *109*, 22–29.

Stewart, C.L. (1993). Production of chimeras between embryonic stem cells and embryos. Meth. Enzymol. *225*, 823–855.

Sugimoto, T., Tanabe, Y., Shigemoto, R., Iwai, M., Takumi, T., Ohkubo, H., and Nakanishi, S. (1990). Immunohistochemical study of a rat membrane protein which induces a selective potassium permeation: its localization in the apical membrane portion of epithelial cells. J. Membr. Biol. *113*, 39–47.

Swanson, R., Hice, R.E., Folander, K., and Sanguinetti, M.C. (1993). The IsK protein, a slowly activating voltage-dependant K+ channel. Sem. Neurosci. *5*, 117–124.

Szabo, P., and Mann, J.R. (1994). Expression and methylation of imprinted genes during in vitro differentiation of mouse parthenogenic and androgenetic embryonic stem cell lines. Development *120*, 1651–1660.

Takumi, T., Ohkubo, H., and Nakanishi, S. (1988). Cloning of a membrane protein that induces a slow voltage-gated potassium current. Science *242*, 1042–1045.

Tesson, F., Donger, C., Denjoy, I., Berthet, M., Petit, C., Bennaeem, M., Coumel, P., Schwartz, K., Barhanin, J., and Guicheney, P. (1996). Exclusion of KCNE1 (IsK) as a candidate gene for Jervell and Lange-Nielsen syndrome. J. Mol. Cell. Cardiol. *28*, 2051–2055.

Tohse, N. (1990). Calcium-sensitive delayed rectifier potassium current in guinea pig ventricular cells. Am. J. Physiol. *258*, H1200–1207.

Tsukahara, Y., Houtani, T., Ueyama, T., Ikeda, M., Nakanishi, S., Yamamoto, A., Tashiro, Y., and Sugimoto, T. (1995). A subpopulation of large ganglion neurons express IsK protein mRNA: an in situ hybridization analysis in the rat eye. Brain Res. Mol. Brain Res. *29*, 376–380.

Wangemann, P. (1995). Comparison of ion transport mechanisms between vestibular dark cells and strial marginal cells. Hearing Res. *90*, 149–157.

Wangemann, P., and Marcus, D.C. (1990). K(+)-induced swelling of vestibular dark cells is dependent on Na+ and Cl− and inhibited by piretanide. Pflugers Arch. *416*, 262–269.

Wangemann, P., and Shiga, N. (1994). Cell volume control in vestibular dark cells during and after a hyposmotic challenge. Am. J. Physiol. *266*, C1046–1060.

Wangemann, P., Liu, J., and Marcus, D.C. (1995a). Ion transport mechanisms responsible for K+ secretion and the transepithelial voltage across marginal cells of stria vascularis in vitro. Hearing Res. *84*, 19–29.

Wangemann, P., Liu, J., Shen, Z., Shipley, A., and Marcus, D.C. (1995b). Hypo-osmotic challenge stimulates transepithelial K+ secretion and activates apical IsK channel in vestibular dark cells. J. Membr. Biol. *147*, 263–273.

Wangemann, P., Shen, Z., and Liu, J. (1996). K+-induced stimulation of K+ secretion involves activation of the IsK channel in vestibular dark cells. Hearing Res., in press.